Study of ICRH scenarios for thermal ion heating in JET D–T plasmas

2012 Nucl. Fusion 52 094012

(http://iopscience.iop.org/0029-5515/52/9/094012)

Nucl. Fusion **52** (2012) 094012 (14pp) doi:10.1088/0029-5515/52/9/094012

Study of ICRH scenarios for thermal ion heating in JET D–T plasmas

Ye.O. Kazakov[1], V.G. Kiptily[2], S.E. Sharapov[2], D. Van Eester[3] and JET EFDA Contributors[a]

JET-EFDA Culham Science Centre, Abingdon, OX14 3DB, UK
[1] Department of Applied Physics, Nuclear Engineering, Chalmers University of Technology, Euratom-VR Association, Göteborg, Sweden
[2] EURATOM-CCFE Fusion Association, Culham Science Centre, UK
[3] LPP-ERM/KMS, Association 'Euratom-Belgian State', TEC Partner, Brussels, Belgium

E-mail: kazakov@nephy.chalmers.se

Received 17 January 2012, accepted for publication 2 July 2012
Published 3 September 2012
Online at stacks.iop.org/NF/52/094012

Abstract
Various ion cyclotron resonance heating (ICRH) scenarios relevant for the D–T phase of the JET tokamak are studied. Recent ICRH experiments in JET (^{3}He)–D and (^{3}He)–H plasmas confirmed the possibility of electron heating enhancement in the mode conversion (MC) regime due to the constructive interference of the reflected fast waves. Such a heating enhancement in D–T plasma is investigated first for JET-like conditions for both dipole and $+\pi/2$ ICRH antenna phasing, and for T concentration varied from 0% to 100%. It is shown that most of the MC scenarios at comparable concentrations of D and T species suffer from a parasitic absorption by fusion-born alpha-particles and NBI-produced fast ions whereas the impact of such fast ions in the minority heating (MH) ICRH schemes is substantially smaller. A possibility of ion heating enhancement due to the interference effect is shown for the MH scenarios. It is found that thermal ion heating becomes dominant in tritium-rich plasmas with T concentration ~80%. The efficiency of ion heating in such a scenario is compared with the alternative ^{3}He minority ICRH scenario in D : T = 50 : 50 plasmas.

(Some figures may appear in colour only in the online journal)

1. Introduction

Ion cyclotron resonance heating (ICRH) is widely used in present-day fusion devices and is foreseen as one of the main heating schemes in the next-step burning plasma ITER experiment [1, 2]. ICRH has a number of advantages among other radiofrequency (RF) methods: technological feasibility of the RF system for this frequency range (f = 20–120 MHz), no density limits for the fast Alfvén (compressional) wave (FW) in accessing the plasma core, good coupling efficiency, and existence of several linear damping mechanisms that gives the flexibility to change the dominant heating to ion or electron species according to the chosen ICRH scenario [3, 4]. ICRH is also one of the most cost effective heating systems envisaged for ITER.

In contrast to fusion-born alpha-particles and MeV-range NBI-produced ions in ITER, which mostly heat electrons, ICRH is the only scheme capable of delivering dominant heating of thermal ions. The use of ion heating scenarios would enhance significantly the fusion reactivity and also could make a bridge to present-day large tokamaks, in which the main heating power from ~100 to 150 keV NBI provides a dominant ion heating.

It is well known that for efficient ICRH at the fundamental cyclotron frequency ($\omega = \Omega_i$) one needs to operate with the plasma consisting of at least two different ion species. Depending on the relative concentration of ion species, two heating regimes are usually distinguished: ion minority heating (MH) and mode conversion (MC) [5]. MH scheme requires a low minority ion concentration which is typically a few per cent (the optimal minority concentration depends on the plasma composition and chosen antenna phasing). In this regime the majority ions provide favourable polarization of the FW at the region of the fundamental cyclotron resonance of the minority ions, which absorb the RF energy and transfer it to bulk plasma particles via collisions leading to either ion or electron heating, depending on the ratio between the minority tail energy, E_{tail}, and the critical energy, $E_{crit} = 14.8 A_f T_e (\sum_i (n_i/n_e) Z_i^2/A_i)^{2/3}$ (here, A_f and A_i are the atomic masses of fast and bulk ions, respectively). With the gradual further increase in the minority concentration the efficiency of the MH becomes less effective

[a] See the appendix of Romanelli F. *et al* 2010 *Proc. 23rd IAEA Fusion Energy Conf. 2010 (Daejeon, Korea, 2010)* http://www-pub.iaea.org/mtcd/meetings/PDFplus/2010/cn180/cn180_papers/ov_1-3.pdf.

and at large enough minority concentrations the MC regime becomes dominant. It is characterized by a partial conversion of the FW to the short wavelength modes, ion Bernstein wave (IBW) and ion cyclotron wave (ICW), at the MC layer which is located between the fundamental cyclotron resonance layers of the ion species, Ω_1 and Ω_2. The converted wave is commonly—but not always—absorbed by electrons within a narrow spatial region. Characterized by fairly localized power deposition profiles, MC has become one of the standard tools for transport analysis [6]. Over the last few years MC heating has been actively studied due to the various applications of this method in current-day tokamaks beyond the heating itself.

Experimental D–T campaigns at JET and TFTR tokamaks evaluated a wide range of ITER relevant ICRH scenarios [7, 8]. The second harmonic tritium scenario is currently considered as the main heating scenario for the activated phase of ITER since it is applicable to D : T = 50 : 50 plasmas [1]. At TFTR, applying additional 5.5 MW of $\omega = 2\Omega_T$ ICRH power in D–T supershots driven by 23.5 MW of NBI, an increase in the central ion temperature from 26 to 36 keV was observed [9, 10]. The best performance achieved with this scheme at JET showed the predominance of electron heating in ICRH-only heated plasmas as expected [7]: ion heating at the harmonics being a finite Larmor radius (FLR) effect involves the waves to interact with the energetic ion populations leading to the strong energy tail generation. The discrepancy between TFTR and JET $\omega = 2\Omega_T$ heating results was due to the combined use of ICRH and NBI at TFTR, while at JET ICRH was applied only.

Deuterium and helium-3 MH were also tested in JET D–T plasmas. Maximum fusion reactivity was observed for deuterium MH with D : T = 9 : 91 plasma [11, 12]. A steady-state burning plasma with $Q = 0.22$ was achieved on JET due to suprathermal fusion reactions between high energy deuterons accelerated by ICRH and the thermal tritium ions. However, the highest central ion temperature and the strongest ion heating were observed at higher D concentration, $X[\mathrm{D}] = n_\mathrm{D}/n_\mathrm{e} = 18\%$ [11, 13]. In such a way, the minority concentration optimal for maximizing the D–T fusion rate is not necessarily optimal for reaching the highest ion temperature showing clearly the difference between the suprathermal and thermal fusion yield.

In the presence of ^{3}He ions, the fundamental ^{3}He minority and second harmonic tritium resonances are two main competing absorption mechanisms since both resonances occur at the same position in plasma. Adding a small amount of ^{3}He into D–T plasma strongly enhances neutron yield [14, 15]. In comparison with the second harmonic T heating, the minority ^{3}He heating is a higher single-pass absorption scheme. In addition, the critical energy for ^{3}He ions is much higher favouring the transfer of the energy from the energetic minority to thermal ions rather than to electrons. At JET, a fourfold increase in the fusion yield was achieved with the injection of some ^{3}He ions, $X[^3\mathrm{He}] = 4\%$, prior to the ICRH [11].

The experimental results obtained in JET D–T campaigns were analysed in [16] using the PION code [17], which self-consistently calculates the power absorption and the development of the fast ion velocity distribution function. In general, a good correspondence between the experimental results and simulations was found. In particular, the predicted fusion reactivity was found to be in an agreement with the observed reactivity. For the MC scenarios it was noted, however, in [16] that a simple Budden estimate of the mode converted power [18] (predicting that up to 25% of the FW energy could be converted only) does not explain the experimental results showing a higher converted power fraction. In TFTR experiments it was also observed that 60–80% of the ICRH power was coupled to electrons via MC [19].

A possible explanation for the observed increased fraction of ICRH power coupled to electrons via MC of the FW to the IBW [9, 16, 19] could be a constructive interference effect, which we consider in this paper. The fraction of the mode converted power is proportional to the square of the RF electric field at the MC layer. Due to multiple FW reflections in the plasma, the spatial electric field pattern changes which can result in higher fraction of FW energy that goes to the short wavelength modes. This effect was first identified in numerical modelling [20]. Later, a triplet theory was developed in [21] showing explicitly that accounting for the high-field side (HFS) FW cutoff ('cutoff-resonance-cutoff' structure), an increase in the MC efficiency by a factor of 4 could be achieved as compared with the isolated 'cutoff-resonance' case considered by Budden. An enhancement of the ICRH MC efficiency due to the constructive interference effect was experimentally validated recently in (^{3}He)–D and (^{3}He)–H JET plasmas [22, 23]. The experimental data of the power absorbed by electrons in the MC regime were found to be an oscillatory function of the minority ^{3}He concentration as predicted by the theory and numerical calculations [21, 24, 25]. This paper aims at exploiting the constructive interference effect for increasing the efficiency of the MC and bulk ion heating in D–T plasma for the conditions of the tokamak JET.

The absorption of ICRH power by fast ion populations (alpha-particles generated in fusion reactions and NBI-produced fast ions) is a limiting factor in the use of ICRH in D–T plasmas [26–28]. A parasitic absorption of ICRH power by these fast ions causes enhanced fast ion losses and increases the power transfer from fast particles to electrons at the expense of a direct bulk ion heating. Aiming at an efficient use of ICRH for heating thermal D–T plasmas, one should optimize the heating scenarios for lower values of the unwanted absorption by alpha-particles and NBI-produced ions.

The paper is organized as follows. Section 2 presents the results of calculations of ICRH power absorption in D–T plasma showing the oscillatory behaviour at varying D : T ratio and the heating enhancement typical of the constructive interference effect. The impact of fusion-born alpha-particles and NBI-produced energetic ions on ICRH power distribution is examined in section 3. Section 4 presents a theoretical model for the heating enhancement in the MH regime which is used for optimizing the MH scenarios for D–T plasma. Section 5 is devoted to studying the D MH in T plasmas. The alternative ^{3}He MH scenario in a balanced D–T mix close to 50 : 50 is evaluated in section 6. Conclusions are drawn in section 7.

2. Heating enhancement in D–T plasma due to the constructive interference effect

For maximizing the constructive interference effect, one has to consider plasma and ICRH plant parameters close to the

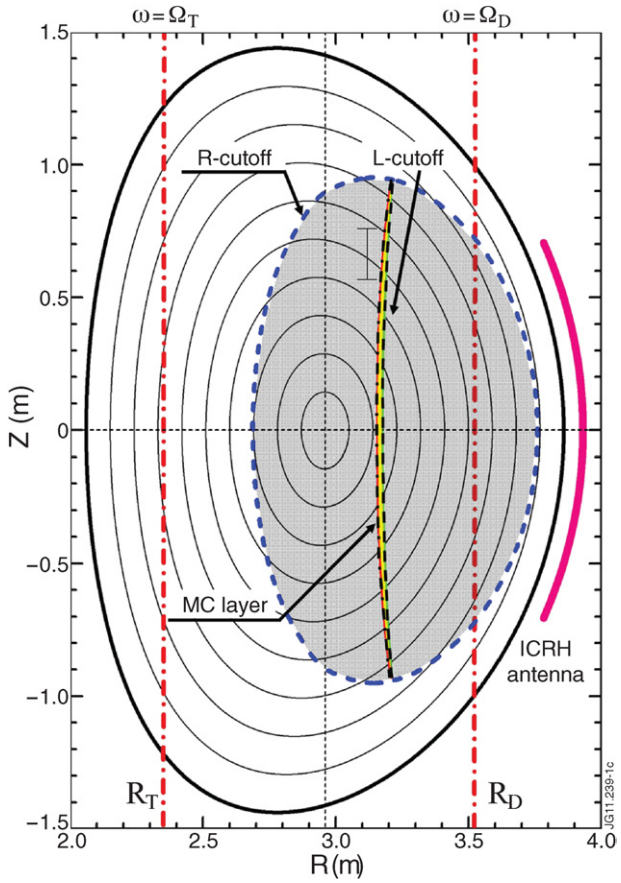

Figure 1. Locations of the fundamental cyclotron resonance layers of deuterium and tritium ions denoted as R_D and R_T with the locations of the MC and fast wave cutoffs layers in the poloidal plasma cross-section, $B_0 = 3.6\,\mathrm{T}$, $f = 23\,\mathrm{MHz}$, $\mathrm{T:D} = 70:30$, $n_\varphi = 27$.

technical limits obtained in D–T experiments on JET [11, 12]. Namely, the RF generator frequency is kept as low as possible ($f = \omega/2\pi = 23\,\mathrm{MHz}$), and the central magnetic field is close to the maximum value, $B_0 = 3.6\,\mathrm{T}$. This set of parameters places both the fundamental cyclotron layers of deuterium and tritium inside the plasma ($R_D = 3.53\,\mathrm{m}$, $R_T = 2.35\,\mathrm{m}$) on an equal distance from the plasma edge (figure 1). Moreover, such a choice of B_0 and f allows one to vary the dominant heating channel (thermal deuterium, tritium or electron species) by adjusting the D : T ratio alone. Central plasma density and temperature are assumed to be similar to those in previous JET experiments: $n_{e0} = 3.0 \times 10^{19}\,\mathrm{m}^{-3}$, $T_{e0} = 7.2\,\mathrm{keV}$, $T_{i0} = 6.6\,\mathrm{keV}$.

The FW propagating in the equatorial plane of the tokamak is fairly well described by the cold-plasma dispersion relation [29]:

$$k^2_{\perp,\mathrm{FW}} = \frac{\omega^2}{c^2}\frac{(L - n^2_\parallel)(R - n^2_\parallel)}{S - n^2_\parallel}, \qquad (1)$$

where $n_\parallel = ck_\parallel/\omega$ is the parallel FW refractive index (the dominant FW $k_\parallel$ is determined by the antenna geometry and chosen antenna phasing). We follow the notation of Stix for the tensor components which for the considered frequency range are given by

$$\begin{aligned} S &\approx 1 + \frac{\omega^2_{\mathrm{pe}}}{\Omega^2_{\mathrm{e}}} - \sum_i \frac{\omega^2_{\mathrm{pi}}}{\omega^2 - \Omega^2_i}, \\ L &\approx 1 + \frac{\omega^2_{\mathrm{pe}}}{\Omega^2_{\mathrm{e}}} + \sum_i \frac{\omega^2_{\mathrm{pi}}}{\Omega_i(\Omega_i - \omega)}, \\ R &\approx 1 + \frac{\omega^2_{\mathrm{pe}}}{\Omega^2_{\mathrm{e}}} + \sum_i \frac{\omega^2_{\mathrm{pi}}}{\Omega_i(\Omega_i + \omega)}, \end{aligned} \qquad (2)$$

where ω_{ps} and Ω_s are the species plasma and the cyclotron frequencies, respectively. The summation in (2) is intended to be taken over all ion species constituting the plasma.

The FW resonance condition $S = n^2_\parallel$ defines the location of the MC layer. Hot plasma theory resolves this resonance and bends it into a confluence. At this layer the FW is partially converted to a short wavelength mode. Generally, there are two types of the mode converted waves, the IBW and the ICW [30–32]. The nature of the short wavelength mode the FW converts into is determined by the competition between the plasma temperature and poloidal magnetic field effects [33]. Near the midplane of the tokamak the FW can couple to the quasi-electrostatic IBW which propagates to the HFS of the conversion region. Having the wavelength of the order of the ion Larmor radius, the IBW commonly heats electrons via Landau damping within a narrow spatial region [34]. Accounting for the finite poloidal magnetic field, one could show that the electromagnetic ICW with the wavelength intermediate between typical FW and IBW exists vertically some distance away from the midplane. ICW, which propagates towards the low magnetic field side (LFS) of the MC region, can be absorbed both by electrons and ions. Interaction of the ICW with the minority ^{3}He ions is suggested to be responsible for driving significant plasma flow, which was observed in (^{3}He)D Alcator C-Mod plasma [35]. Since the existence of the ICW is directly related to the upshifts in $k_\parallel$ induced by the poloidal magnetic field which is a 2D effect, for simplicity reasons in this paper we restrict our analysis considering the conversion of the FW to the IBW.

The MC layer is accompanied closely to the LFS by the left-hand polarized cutoff (L-cutoff) given by the condition $L = n^2_\parallel$. Together, they form the evanescence layer—a region where $k^2_{\perp,\mathrm{FW}} < 0$—which is a barrier for the FW propagation. The fraction of the FW energy converted into the IBW essentially depends on the evanescence layer width which almost linearly depends on the minority concentration.

In addition to L-cutoff, the FW dispersion relation (2) predicts the right-hand polarized cutoffs (R-cutoffs) defined by $R = n^2_\parallel$. These cutoffs, one located at the LFS and the other at the HFS, are much more density profile dependent than L-cutoff which, in turn, depends mostly on the minority concentration.

Figure 1 also shows the location of the MC and fast wave cutoffs layers for the tritium concentration $X[\mathrm{T}] = n_T/n_e = 70\%$ and toroidal wavenumber $n_\varphi = 27 (k_{||} = n_\varphi/R)$ which is dominant for the dipole phasing of A2 ICRH antenna at JET [36]. The shaded area represents a region where the FW is a propagative mode, i.e. $k^2_{\perp,\mathrm{FW}} > 0$.

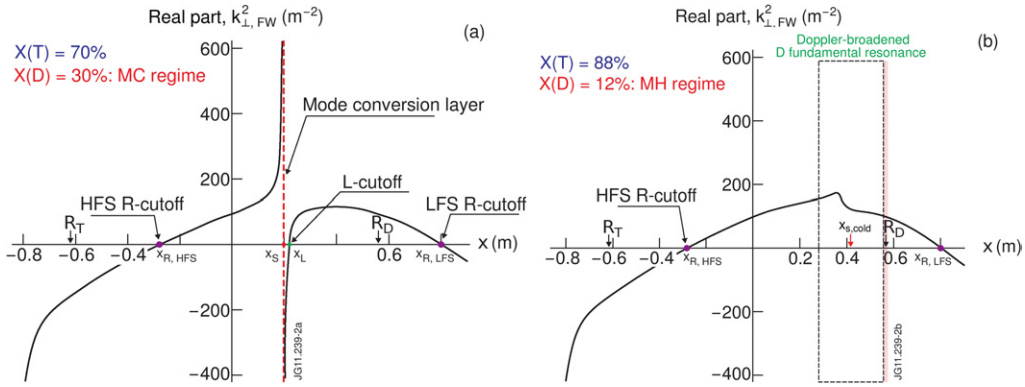

Figure 2. Dispersion of the FW (hot-plasma model) propagating in the equatorial plane (the parameters are given in the main text and caption of figure 1): (*a*) X[D] = 30% (MC regime), (*b*) X[D] = 12% (MH regime).

The FW dispersion relation (the real part of the square of the perpendicular wavenumber, $k^2_{\perp,\mathrm{FW}}$) for the wave propagating in the equatorial plane is shown in figure 2. R-cutoff located at the LFS edge $x_{\mathrm{R,LFS}}$ complicates the coupling of the RF energy from ICRH antenna to the plasma [37]. The FW—as a carrier of the RF energy—must first tunnel through the evanescence layer in front of the antenna before it starts its propagation in the plasma. An extensive ICRH coupling physics analysis and identification of the optimum plasma edge density profile were studied recently in [38]. Reaching the plasma centre, the FW is partially reflected from L-cutoff, x_{L}. By tunnelling part of the FW is transmitted through the MC layer, x_{S}, which is then reflected back from R-cutoff at the HFS, $x_{\mathrm{R,HFS}}$. The FW reflected from the HFS R-cutoff tunnels through the MC layer without supplementary reflection. As a result, the total reflection and, thus, absorption coefficients depend on the amplitudes and phases of these two reflected fast waves.

Provided the reflected waves have equal amplitudes and opposite phases, the reflection coefficient is diminished resulting in turn in the MC enhancement. Analytical formula for the conversion coefficient (and subsequently, for electron heating provided direct electron damping of the FW and minority ion absorption are negligible) in such a structure known as a triplet configuration was derived in [21]:

$$P_{\mathrm{e}} = 4T(1-T)\sin^2(\Delta\phi/2), \qquad (3)$$

where $T = \mathrm{e}^{-\pi\eta}$ is the transmission coefficient through the MC layer, and $\Delta\phi$ is the phase difference between two reflected waves (determined mostly by the distance between the MC layer and the HFS R-cutoff relative to the FW wavelength). The tunnelling factor, η, which roughly equals the product of the FW perpendicular wavenumber (density dependent) by the width of the conversion layer, defines the accessible maximal level of the converted power. It depends on most of the plasma parameters, such as plasma density, minority concentration and magnetic field. The tunnelling factor is also particularly sensitive to the FW toroidal wavenumber [20, 39]. At JET, the ICRH A2 antenna consists of four vertical current straps which can be phased individually $\pm 180^\circ$ with respect to a phase reference signal. Varying the phase difference between the currents in two adjacent straps, different antenna spectra can be employed. As shown in figure 3(*a*), changing the antenna phasing from the dipole ($n_\varphi = 27$) to $+\pi/2$ phasing ($n_\varphi = 14$) results not only in the increase in the MC layer width by a factor of 2, but it also leads to a pronounced shift of the HFS R-cutoff towards the edge extending largely the region of the FW propagation in the plasma. Figure 3(*b*) shows the locations of the MC and cutoff layers as a function of the tritium concentration. It is clear that as the tritium concentration increases, the MC layer shifts towards the minority D cyclotron resonance located at the LFS. Since the radial location at which peak electron power deposition is observed almost coincides with the MC layer [19], the location of the deposition of the RF power in the plasma for MC heating can be changed by modifying the D : T ratio. In contrast, the locations of R-cutoffs in the plasma are almost unaffected with changing X[T]: they are defined mostly by the FW parallel wavenumber (figure 3(*a*)) and the edge plasma density profile.

ICRH absorption efficiency has been evaluated with the 1D full-wave code TOMCAT [40]. This code solves a 12th order wave equation system accounting for the toroidal curvature of the tokamak, but omitting the finite poloidal magnetic field effects, and thus excluding MC of the FW to the ICW. Incorporating up to dominant third harmonic cyclotron heating effects, TOMCAT retains up to second order Larmor radius terms in the operator either acting on the electric field or on the test function vector in the weak Galerkin form of the wave equation and hence has up to fourth order Larmor radius terms and fourth derivatives acting on each of the electric field components in the corresponding dielectric tensor. This raises the order of the wave system from the usual 6 to 12 but guarantees a positive definite and purely resonant absorption for Maxwellian populations for any of the retained waves [22]. The imposed boundary conditions correspond to the pure excitation of the FW from the LFS of the tokamak. TOMCAT gives scattering coefficients (reflection, transmission, conversion and absorption) for a double transit of the FW over the plasma. In contrast to usual full-wave codes where all the RF power launched into the plasma is assumed to be absorbed (i.e. multi-pass absorption), TOMCAT gives the absorption coefficients for a double sweep. The evaluation of a douple-pass absorption coefficient allows one to estimate qualitatively the heating efficiency of the studied ICRH scenario. However, this gives only qualitative results since a number of effects are omitted in 1D geometry. More rigorous treatment of the FW propagation and MC in tokamaks

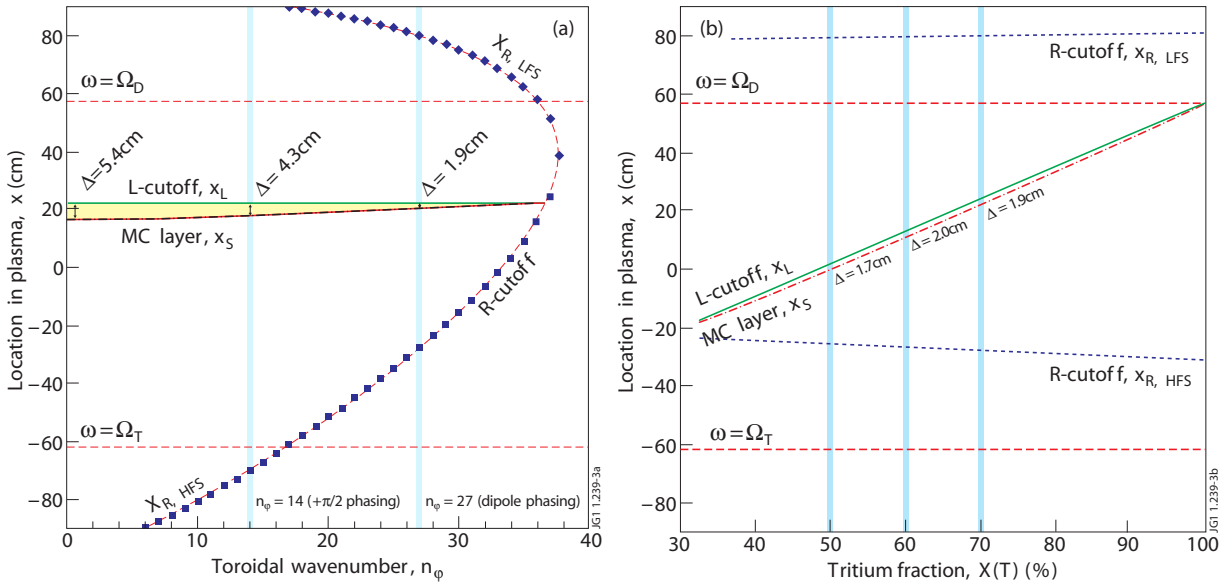

Figure 3. (*a*) Locations of the FW cutoffs and MC layer versus the toroidal wavenumber, X[D]= 30%. (*b*) Locations of the FW cutoffs and MC layer versus the tritium fraction, $n_\varphi = 27$.

should be essentially based on the 2D full-wave modelling, e.g. [41–43].

Figures 4(*a*) and (*b*) show the computed dependence of the double-pass absorption coefficients as a function of the tritium concentration for $n_\varphi = 27$ and $n_\varphi = 14$, respectively. By varying X[T], one changes the transparency of the MC layer (which defines maximal absorption) as well as the distance between the MC layer and the HFS R-cutoff, hence, modifying the interference phase conditions (figure 3(*b*)). As predicted by equation (3), the absorption coefficients vary oscillatory with the change of X[T]. For $n_\varphi = 27$ there are three pronounced maxima achieved at X[T] = 44%, X[T] = 69% and X[T] = 88%. The first two correspond to the MC regime and give rise to electron heating. The third maximum at X[D] = 12% corresponds to the MH ion regime. For $n_\varphi = 14$ absorption curves have a large number of maxima since for this phasing the HFS R-cutoff is located far closer to the edge.

In appendix A it is shown that the normalized double-pass absorption coefficients evaluated with TOMCAT for the considered heating scenario with $n_\varphi = 27$ are compatible with the more sophisticated modelling using the 2D full-wave TORIC code [42]. The distribution of the RF power between the plasma species, ions and electrons, as a function of the tritium concentration, is found to be similar though the interference effect is less pronounced in 2D geometry. It goes without saying that 1D modelling could be used only for qualitative calculations helping one to assess the wave physics for the heating scenarios of interest and estimating the range of optimal plasma parameters. Accounting for the real 2D geometry—upon a summation over all coupled poloidal modes—the wave interference effect is moderated to what should be expected from a 1D description. A question of how much the interference pattern is smoothened in 2D geometry, particularly, upon accounting for different toroidal wavenumbers in the antenna spectrum, is a subject of a separate future paper.

Summarizing the results of this section, we conclude that according to figures 4(*a*) and (*b*) it is possible to tune the plasma parameters in such a way to provide high values for the double-pass ICRH absorption coefficients in D–T plasma (both for the MC and the MH regimes) due to the additional reflection of the FW from the HFS R-cutoff. However, this modelling excludes any fast ion populations in D–T plasma, such as NBI-produced fast ions and fusion-born alpha-particles, the effect of which on RF power absorption will be the subject of the next section.

3. Effect of fast particles on ICRH power distribution

In order to achieve fusion-relevant plasma temperatures several auxiliary heating methods are commonly used simultaneously [1]. NBI heating relies on the injection of the neutral particles of high energies into the plasma where they are ionized and transfer their energy to ions or electrons via collisions. NBI has been routinely used both for heating and fuelling the plasma. For instance, JET is equipped with two NBI modules which accelerate D particles up to the 130 keV [44]. In this paper, a qualitative investigation of the effect of non-thermal subpopulations of ions is given for ICRH scenarios. All species (including fast ions) are assumed to be Maxwellian with a certain effective temperature [27]. This constraint condition is imposed in many ICRH full-wave solvers. More rigorous description requires coupling of ICRH solver with Fokker–Planck or orbit-following Monte Carlo code to evaluate the heating profiles and particle distribution function in a self-consistent way [45–48]. This, however, is far beyond the scope of this paper.

Figures 4(*c*) and (*d*) show that adding a small subpopulation of 1% of NBI-produced fast D ions with the effective temperature 55 keV [47] dramatically diminishes the efficiency of electron heating in the MC regime. Although the total absorption efficiency remains unchanged, the distribution of the RF power is different. Most of the RF power in the MC regime is absorbed by fast ions because of the large Doppler-shift of their resonance. For thermal particles this shift is small,

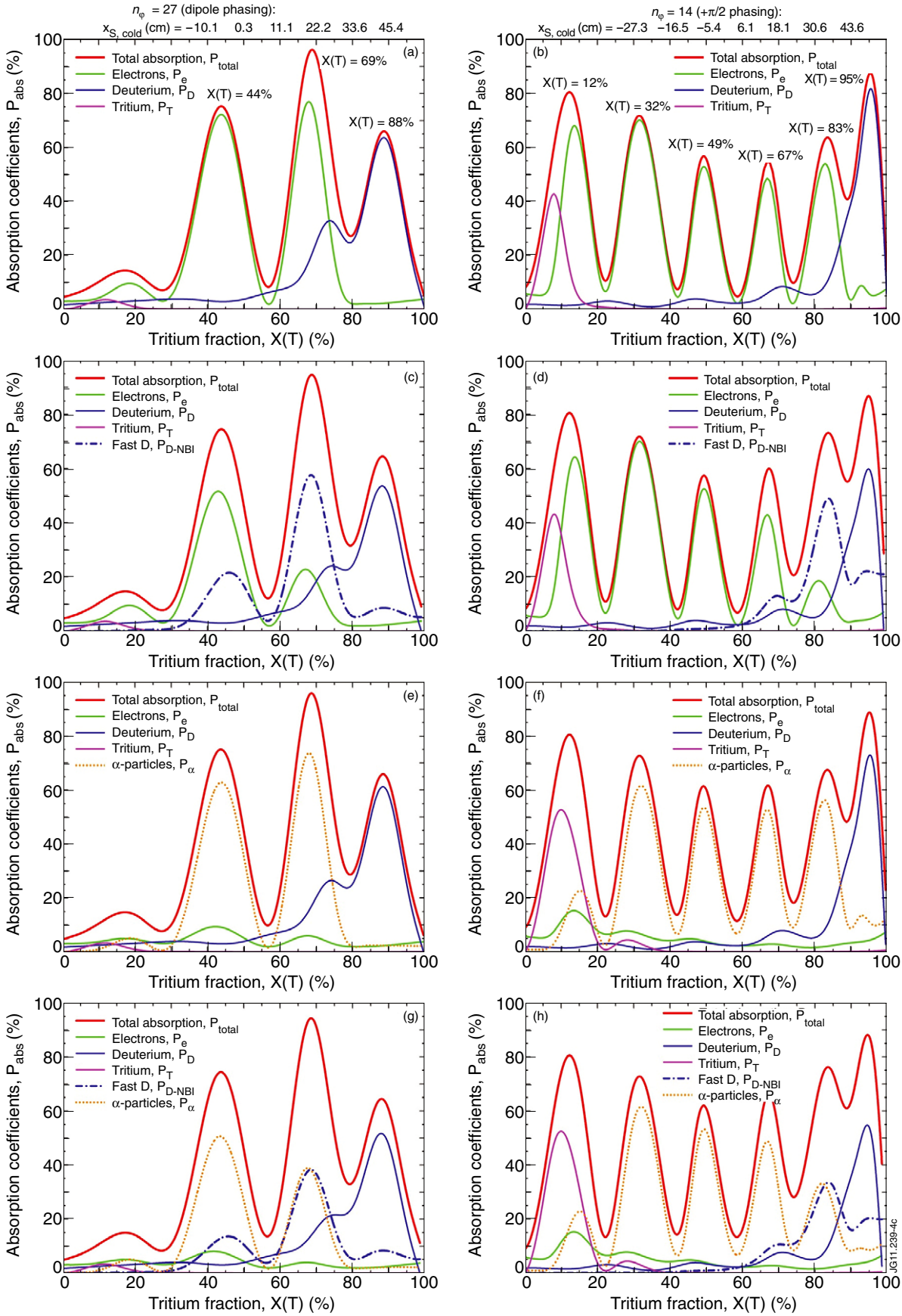

Figure 4. Double-pass absorption coefficients versus the tritium concentration. Left figures are calculated for $n_\varphi = 27$, right figures for $n_\varphi = 14$. (*a*), (*b*) No fast particles; (*c*), (*d*) NBI D beam, $X[\mathrm{D_{NBI}}] = 1\%$, $T_{\mathrm{eff},0} = 55$ keV; (*e*), (*f*) alpha-particles, $X[\alpha] = 0.2\%$, $T_{\mathrm{eff},0} = 1.12$ MeV; (*g*), (*h*) NBI D beam + alpha-particles.

so these particles absorb the RF power close to their cyclotron resonance layer. In contrast, fast particles can absorb the RF energy far from the cold ion cyclotron region resulting in broad RF deposition profiles. Note that for the conditions of the MH maximum ($X[\mathrm{D}] = 12\%$) the effect of D beam on the RF power distribution is much weaker.

The interaction of fast NBI ions with ICRH was identified earlier at different tokamaks [34, 49–51]. D beam ion heating by ICRH was successfully implemented in recent experiments on fundamental RF heating of JET deuterium plasmas [47, 51]. The obtained results suggest that NBI-produced fast ions could be accelerated to the energies much higher than their initial birth energy. The synergy between NBI and ICRH could lead to a strong redistribution and the enhanced losses of fast particles accelerated to MeV energies which were experimentally demonstrated in (^{3}He)–D plasma [22, 52].

The parasitic absorption of ICRH power by alpha-particles is another significant effect to be considered for ICRH in D–T plasma [26–28]. Similar to NBI-produced fast D ions, alpha-particles with the same charge-to-mass ratio as D ions—as soon as they are born in D–T fusion reactions—should provide an even more significant effect on RF power distribution. Although it is difficult to make self-consistent calculations of such an effect accounting for the dielectric tensor modification and the complicated distribution function of fast ions, good qualitative estimates could be obtained by representing alpha-particles as Maxwellian population with an effective temperature 1.12 MeV [27]. Taking into account the typical values of alpha-particle density in JET D–T discharges (see, e.g. [53]), we assume $X[\alpha] = 0.2\%$ throughout in our calculations. Figures 4(*e*) and (*f*) confirm that the considered ICRH scenarios suffer from the unwanted absorption by alpha-particles in a wide range of D : T concentrations. Results for D–T mix with both D beam and alpha-particles (figures 4(*g*) and (*h*)) show that they absorb comparable fractions of the RF energy. These figures show that only for T rich plasma (for the conditions considered one needs $X[\mathrm{T}] > 80\%$ for the dipole phasing, and $X[\mathrm{T}] > 90\%$ for the $+\pi/2$ phasing) the effect of fast particles on the RF power distribution is quite low.

Figure 4 suggests that the absorption coefficient by minority species in the MH regime has also an oscillatory nature (there is a secondary minority ion absorption maximum though less pronounced). Below we confirm that the high levels of the minority ion absorption could be achieved even for moderate values of the single pass absorption (40–60%) due to the constructive interference effect. This effect is similar to the electron heating enhancement in the MC regime identified earlier [20, 21]. If comparing absorption curves for dipole and $+\pi/2$ phasings, one can clearly see that the tritium concentration at which the transition from the MH to MC regime occurs is almost twice as high for the dipole phasing. This is consistent with the predictions for the critical minority concentration presented in [54]. According to [55], the minority tail energy reached is inversely proportional to the minority concentration. In such a way, high concentration D minority ICRH with dipole phasing is beneficial in view of improving the bulk ion heating in D–T plasmas [56].

4. Ion heating enhancement in the MH regime

It was previously shown in [20, 21, 25], that due to the additional reflection of the FW from the HFS R-cutoff or the supplementary MC layer significant improvement of the electron heating is possible. The interference effect could be used to increase not only electron heating in the MC regime, but to maximize the ion heating enhancement in the MH regime as well.

We apply similar logic to that described in [21, 25] to explain the ion heating enhancement in the MH regime caused by the additional reflection of the FW from the HFS R-cutoff (figures 4(*a*) and (*b*)). First, consider the distribution of RF power in a system without R-cutoff. Then, while propagating through the Doppler broadened minority fundamental resonance layer ($\omega \approx \Omega_{\mathrm{mino}}$), part of the FW energy is transmitted, T and part of the energy is absorbed, P_1 which is usually referred to as a single-pass absorption coefficient. In addition to that spatial variation of the FW perpendicular wavenumber within the broadened minority cyclotron layer (figure 2(*b*))—particularly, at the region corresponding to the cold plasma hybrid resonance (for MH regime it is located within the Doppler broadened cyclotron resonance)—causes a small non-zero fraction of the FW energy to be reflected at the cyclotron resonance [57, 58]. This is schematically shown in figure 5(*a*) (see also appendix B). Usually being very small ($R \simeq 5\%$), this reflection plays a minor role in a single-pass transit. But for a double-pass transit, this non-zero reflection is a key condition for ion heating enhancement.

Figure 5(*b*) shows that if the HFS R-cutoff is present in the plasma, then the transmitted wave is reflected back to the plasma centre. After transmitting through the resonance layer, the FW field pattern at the LFS is determined by the interference of two reflected waves. The amplitude of the wave reflected directly from the minority cyclotron layer is $r_1 = \sqrt{R}\,\mathrm{e}^{\mathrm{i}\phi_1}$, and the amplitude of the second wave originated due to the reflection from the HFS R-cutoff is $r_2 = T\,\mathrm{e}^{\mathrm{i}\phi_2}$ (the transmission coefficient does not depend on the wave incidence side). In such a way, the resulting power reflection coefficient is given by

$$R_{\mathrm{sum}} = |r_1 + r_2|^2. \tag{4}$$

After some algebra, one can prove that in such a system (figure 5(*b*)) a double-pass absorption coefficient for minority ions is equal to

$$P_{\mathrm{i}} = P_{\mathrm{min}} + 4T\sqrt{R}\sin^2(\Delta\phi/2). \tag{5}$$

Depending on the value of the phase difference between the reflected waves $\Delta\phi = \phi_2 - \phi_1$, a double-pass absorption coefficient for minority ions varies between the maximal (P_{max}) and minimal (P_{min}) levels corresponding to limiting cases of the constructive and destructive wave interference, respectively. In terms of single-pass scattering coefficients they are given by the expressions

$$P_{\mathrm{min}} = 1 - (T + \sqrt{R})^2 = P_1 + T(1 - T - 2\sqrt{R}), \tag{6}$$

$$P_{\mathrm{max}} = P_{\mathrm{min}} + 4T\sqrt{R} = P_1 + T(1 - T + 2\sqrt{R}).$$

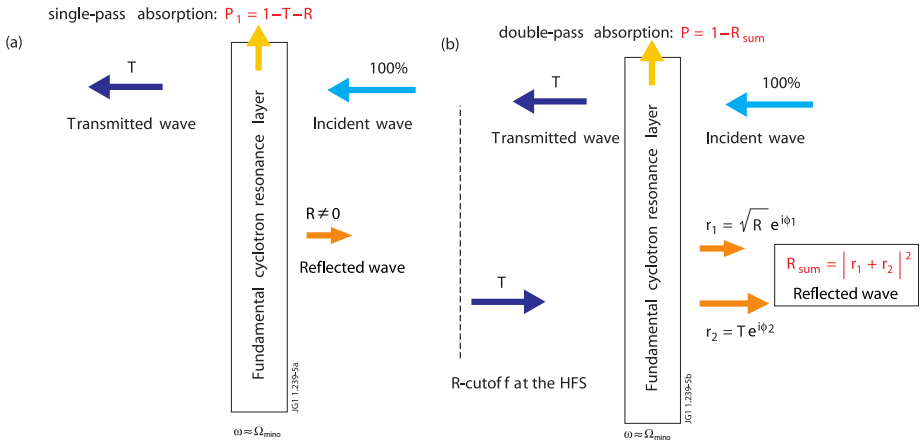

Figure 5. The enhancement of the ion heating in the MH regime is also possible due to the additional reflection of the FW from the HFS R-cutoff. (*a*) Crossing the Doppler broadened minority cyclotron resonance layer $\omega \approx \Omega_{\text{mino}}$, the FW is not only partially absorbed and transmitted, but there is also a finite reflection of the wave, $R \neq 0$. (*b*) MH enhancement is caused by the interference of the fast waves reflected at the cyclotron resonance and HFS R-cutoff.

If the reflection coefficient for a single pass of the FW through the resonance layer equals $R = (1 - T)^2$ (this case corresponds to the isolated Budden cutoff-resonance layer), then formula (5) reduces to that obtained by Fuchs *et al* [21] for electron heating via FW to IBW MC: $P_{\min} = 0$, $P_{\max} = 4T(1 - T)$, $P = 4T(1 - T)\sin^2(\Delta\phi/2)$. However, for the ion heating scenarios the reflection coefficient, R, is usually only a few per cent. Hence, for the given P_1 and T the ion absorption coefficient varies from its minimal, $P_{\min}$, to its maximal, $P_{\max}$, value defined by equation (5) depending on the exact value of the phase difference, $\Delta\phi$. As shown later, even a small reflection of the FW from $\omega \approx \Omega_{\text{mino}}$ resonant layer at the level 3–5% could lead to the increase in the ion heating efficiency by ~40–50%. This effect was numerically shown in [22, figure 2(*a*)], where a pronounced maximum at $X[^3\text{He}] = 8\%$ gave rise to an efficient minority ion heating in (^{3}He)–D plasma.

Figure 6 shows the double-pass absorption coefficient for the minority ions P_2 calculated from equation (5) and accounting for the interference of the reflected fast waves as a function of the single-pass absorption coefficient P_1. The dashed line corresponds to P_1. The dashed–dotted line represents the double-pass absorption coefficient assuming $R = 0$. It is higher than P_1 since the additional fraction of the FW energy, $P_1(1 - P_1)$, is absorbed during the second pass of the FW through the resonance layer. Solid curves in figure 6 (red and green) define the maximal and minimal values of P_2 for $R = 5\%$ accounting for the interference of the waves. For example, if the single-pass absorption equals 40%, then as follows from equation (5) $P_{2,\min} = 40.2\%$ and $P_{2,\max} = 89.3\%$. In such a way due to the additional FW reflection from the HFS R-cutoff and a finite reflection of the FW from the minority resonance layer at the level 5%, the resulting absorption coefficient for the minority ions could increase by 50%. The constructive interference effect gives a possibility to increase significantly the double-pass ion absorption coefficient for ICRH MH scenarios with a moderate single-pass absorption by tuning the plasma parameters in a proper way.

In the next two sections we evaluate two ICRH scenarios which have (i) good ion heating efficiency due to the constructive interference effect; (ii) low impact of fast ions on the RF power absorption. The first is the (D)–T scheme with dominant absorption by D minority ions. The second is the (^{3}He)–DT scenario in which most of the RF energy is absorbed by ^{3}He minority ions in a balanced D–T mix.

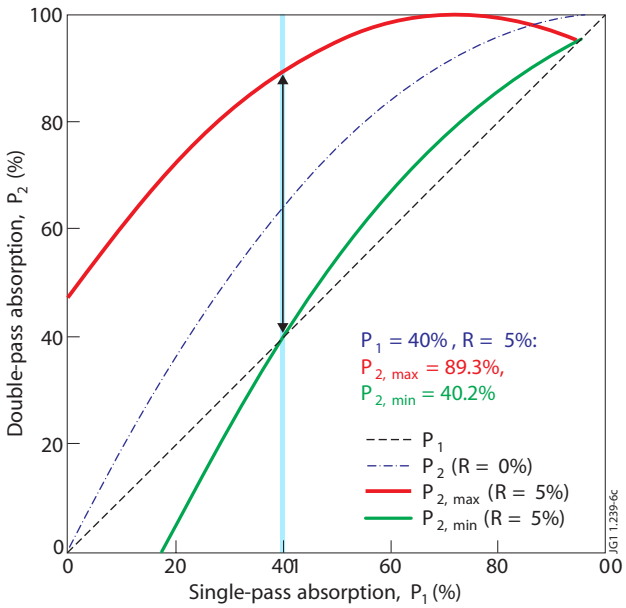

Figure 6. Minimal and maximal levels of the double-pass minority absorption coefficient, P_2 (accounting for the interference of the waves) as a function of the single-pass absorption coefficient, P_1.

5. (D)–T MH scenario: X[D] = 20%

As follows from figure 4, efficient minority ion heating can be achieved in a range $X[\text{D}] = 5$–25%, which is in agreement with experimental results [11, 12]. Consider (D)–T ICRH scenario with the following plasma parameters: T : D = 4 : 1 mix, $n_\varphi = 27$ (dipole phasing as noted before allows one to operate with higher minority concentrations), $B_0 = 3.6$ T, $f = 24$ MHz (somewhat higher frequency is used than that

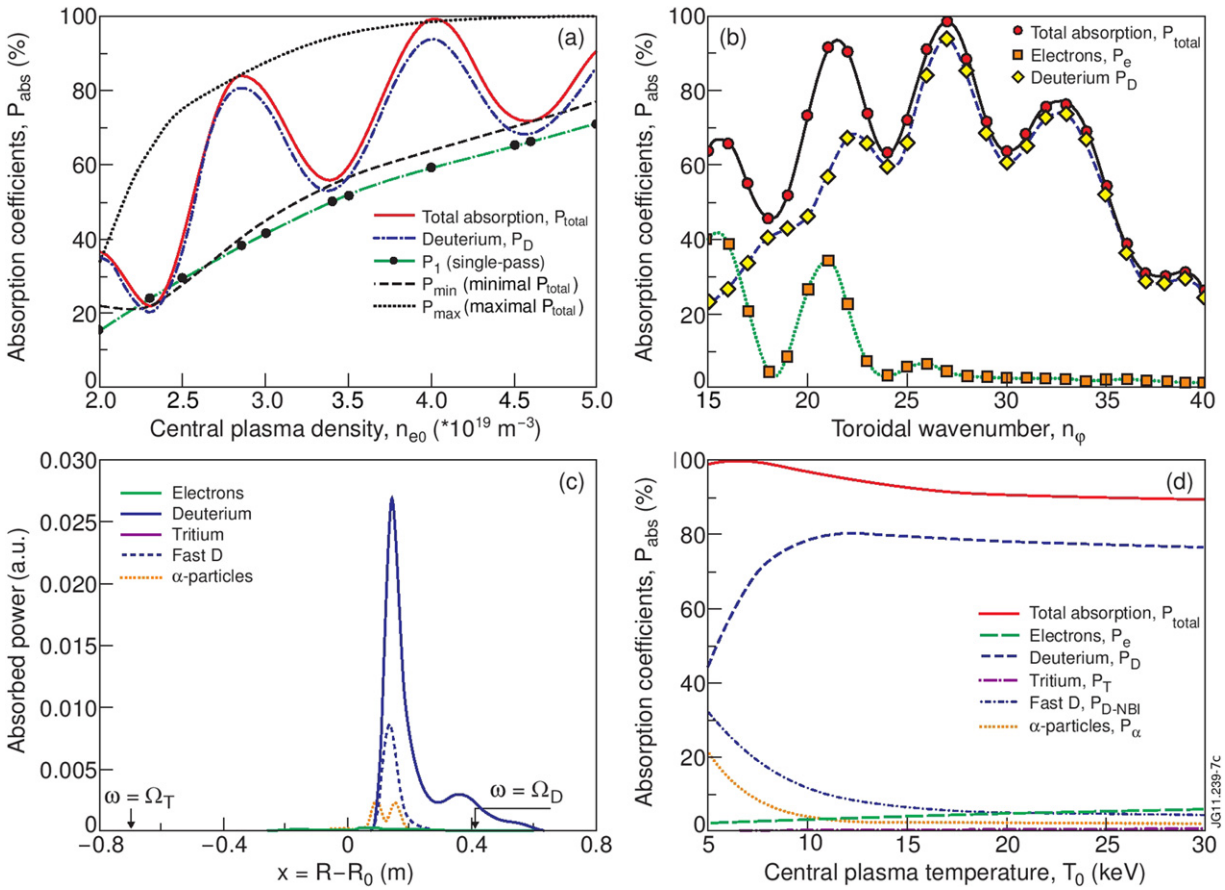

Figure 7. TOMCAT results for (D)-T ICRH scenario, T : D= 4 : 1, $n_\varphi = 27$, $f = 24$ MHz, $B_0 = 3.6$ T, $T_0 = 8$ keV. (*a*) Absorption coefficients (without fast particles) versus the central plasma density; (*b*) absorption coefficients (without fast particles) versus the toroidal wavenumber for $n_{e0} = 4.0 \times 10^{19}$ m^{-3}; (*c*) ICRH power deposition profiles (with fast particles) for $n_\varphi = 27$, $n_{e0} = 4.0 \times 10^{19}$ m^{-3}; (*d*) absorption coefficients (with fast particles) versus the central plasma temperature for $n_\varphi = 27$, $n_{e0} = 4.0 \times 10^{19}$ m^{-3}.

for figures 1–4, which allows one to locate the ion heating region closer to the plasma centre). For simplicity, in further modelling all plasma species are assumed to have the same central temperature $T_0 = 8$ keV.

Figure 7(*a*) shows the dependence of the double-pass absorption coefficients as a function of the central plasma density calculated with TOMCAT. Table 1 summarizes the numerical and theoretical results for the ion heating efficiency. P_{total} and P_1 are the fractions of the launched wave power absorbed in a double and single pass of the FW over the plasma evaluated numerically. As follows from the table and the figure, theoretical values predicted by formulae (5) and (6) are in a good agreement with the results calculated numerically. The minority ion heating coefficient varies oscillatory as expected. For example, for $n_{e0} = 4.0 \times 10^{19}$ m^{-3} the double-pass absorption coefficient for ions reaches ~100% whereas the single-pass absorption is ~60% only. At central plasma density $n_{e0} = 3.4 \times 10^{19}$ m^{-3} the minimum in total and ion absorption is observed since the phase difference $\Delta\phi$ has decreased by the value of π due to the change in the R-cutoff location and average value of the FW perpendicular wavenumber (for details, see appendix B).

Figure 7(*b*) shows how the absorption coefficients depend on the toroidal wavenumber for the considered central plasma density. Again, they are the oscillatory functions of this parameter, since varying n_φ one changes the location of the HFS R-cutoff (figure 3(*a*)) affecting the phase difference of the reflected waves $\Delta\phi$, which defines the constructive/destructive nature of the interference for any particular case.

The ICRH power deposition profiles for this scenario with $n_{e0} = 4.0 \times 10^{19}$ m^{-3} accounting for the presence of fast particles ($X[D_{NBI}] = 1\%$, $X[\alpha] = 0.2\%$) are shown in figure 7(*c*). In contrast to the MC scenarios (figure 4), where the parasitic absorption almost diminishes electron absorption, for the considered scenario minority D ions are still the main channel of heating: $P_{total} = 98.4\%$, $P_D = 72.0\%$, $P_{D\text{-}NBI} = 16.8\%$, $P_\alpha = 6.8\%$, $P_e = 2.8\%$. Most of the RF power is absorbed by the thermal D ions, whereas the parasitic absorption by D beam and alpha-particles contributes in sum ~24%.

It is important to clarify how the ICRH power distribution varies with the subsequent increase in the plasma temperature to evaluate the effect of fast particles for reactor-relevant temperatures. Figure 7(*d*) shows the dependence of the absorption coefficients as a function of the central plasma temperature for the given set of parameters. It is clearly seen from the figure that with the increase in T_0, the parasitic absorption further decreases. For $T_0 > 15$ keV its contribution to the total absorption is less than 10%. In such a way, this scheme has a better performance for the pre-heated plasmas

Table 1. Absorption coefficients for (D)–T MH scenario. $P_{\rm total}$ and P_1 are the fractions of the launched wave power absorbed in a double and single pass of the FW over the plasma evaluated with the TOMCAT code. Theoretical results predicted by formulae (5) and (6) are in good agreement with the double-pass absorption coefficients calculated numerically.

			Double-pass absorption		Single-pass absorption			Formulae (6)	
n_{e0} (10^{19} m^{-3})	$x_{\rm R,\ HFS}$ (cm)		$P_{\rm total}$	$P_{\rm D}$	P_1	T	R	$P_{\rm min}$	$P_{\rm max}$
2.3	−17.3	**Min**	**22.0%**	20.4%	24.0%	73.5%	2.5%	**20.2%**	66.7%
2.85	−29.0	**Max**	**84.2%**	81.0%	38.4%	58.1%	3.5%	41.0%	**84.5%**
3.4	−37.0	**Min**	**56.0%**	53.0%	50.1%	45.2%	4.7%	**55.3%**	94.5%
4.0	−43.4	**Max**	**99.4%**	94.5%	59.3%	34.0%	6.7%	64.1%	**99.3%**
4.6	−48.3	**Min**	**71.9%**	67.9%	66.2%	26.5%	7.3%	**71.4%**	100%

(for example, using NBI heating at the initial stage) with plasma temperatures $T_0 > 10$ keV.

Since this ICRH scenario could be effective for such high D minority concentration as ∼20%, one should expect that the heated minorities will distribute their energy dominantly to bulk ions favouring to increase the thermal fusion yield in D–T plasmas.

6. (^{3}He)–DT MH scenario: $X[^3\mathrm{He}] = 3.5\%$

For the activated phase of ITER the main operation ICRH scenario foreseen is the second harmonic tritium absorption [1]. However, for typical conditions of JET the absorption efficiency of this scheme is rather low. As discussed in the introduction, adding a small fraction of ^{3}He ions in D–T plasma can significantly improve ion heating efficiency and fusion yield. Using ^{3}He ions as a minority instead of the commonly used H minority is beneficial due to the higher collisionality of ^{3}He ions: the value of the critical energy for ^{3}He ions below which the power flows from the fast ions mainly to the thermal ions is $E_{\rm crit}(^3\mathrm{He}) \simeq 24.8T_e$, which is much higher than that for H ions, $E_{\rm crit}(\mathrm{H}) \simeq 8.3T_e$. Thus, the fast ^{3}He tail accelerated with ICRH favours the collisional transfer of energy from ^{3}He to bulk ions rather than electrons.

Consider the following scenario: $X[^3\mathrm{He}] = 3.5\%$, balanced D–T mix, $f = 34$ MHz (now, the antenna frequency chosen is almost optimal for JET RF power generators), $B_0 = 3.6$ T, $n_\varphi = 27$, $T_0 = 6$ keV. Figure 8(*a*) shows that for the considered conditions minority absorption is maximal at $n_{e0} = 3.6\times10^{19}$ m^{-3}: $P_{\rm total} = 88.7\%$, $P_{3_{\rm He}} = 75.5\%$, i.e. most of the RF energy is absorbed by minority ^{3}He ions in a narrow region close to the plasma centre (figure 8(*c*)). Figure 8(*b*) shows the constructive/destructive interference effect in such a plasma manifested scanning the ion heating efficiency over the toroidal wavenumber.

Although the location of ^{3}He fundamental and T second harmonic layers coincides, tritons absorb only a few per cent of the RF energy. Figure 8(*d*) shows the absorption coefficients as a function of the central plasma temperature. It is clearly seen that in this ICRH scenario fast particles also provide a low impact on the RF power distribution regardless T_0. ^{3}He ion heating efficiency varies between 60% and 70% in a wide range of plasma parameters. Thus, we confirm that ICRH scenario with ^{3}He minority in a balanced D–T mix is one of the best scenarios for tokamaks [11, 14, 15].

7. Conclusions

ICRH scenarios relevant for the activated D–T phase of JET operation are studied qualitatively using the 1D full-wave code TOMCAT. Aiming at the optimization of the existing ICRH systems, recent theoretical and experimental developments in the heating efficiency improvement are employed to maximize the absorption for the considered schemes. The method relies on the RF electric field pattern modification due to multiple fast wave reflections over the plasma. Heating enhancement due to the constructive interference effect has been assessed by calculating numerically the absorption coefficients for varying plasma parameters: minority concentration, plasma density and temperature, toroidal wavenumber, etc.

The calculations have shown that by properly choosing the plasma parameters it is possible to achieve high double-pass ICRH power absorption coefficients for a wide range of D : T concentrations. Since in addition to fuel ions D–T plasma includes non-zero fraction of alpha-particles born in fusion reactions and NBI-produced fast ions, the effect of fast particles on the RF power distribution has been evaluated. It is found that most of the RF power in the mode conversion D–T scenarios is absorbed by fast ion populations rather than bulk particles. This makes applying of the ICRH power in a balanced D–T mix unlikely to be efficient for the thermal plasma heating. Simultaneously, it is shown that the parasitic absorption by fast ions is substantially lower in the minority heating regime.

It is proved that in addition to electron heating enhancement via mode conversion identified earlier in 1D theory and numerical modelling (see, [20, 21]), minority ion heating is also affected by the interference of the multiple reflected fast waves. Within the simplified slab model considered, this allows one to increase ion absorption for the heating scenarios with relatively low single-pass ion damping. It is shown that due to the finite reflection of the FW from the minority cyclotron layer and additional reflection of the FW from the HFS R-cutoff, the minority double-pass absorption coefficient could increase by ∼50%. Analytical formulae for the minority ion absorption coefficient are found, which are in good agreement with the numerical results.

Two ICRH minority heating scenarios are evaluated with TOMCAT and optimized for reaching the enhanced minority ion absorption, which could be used to achieve dominant thermal ion heating in JET D–T plasmas. It is shown that (D)–T minority heating could be effective for such high D minority concentrations as ∼20% being beneficial for lowering the minority tail energy and increasing thermal fusion yield.

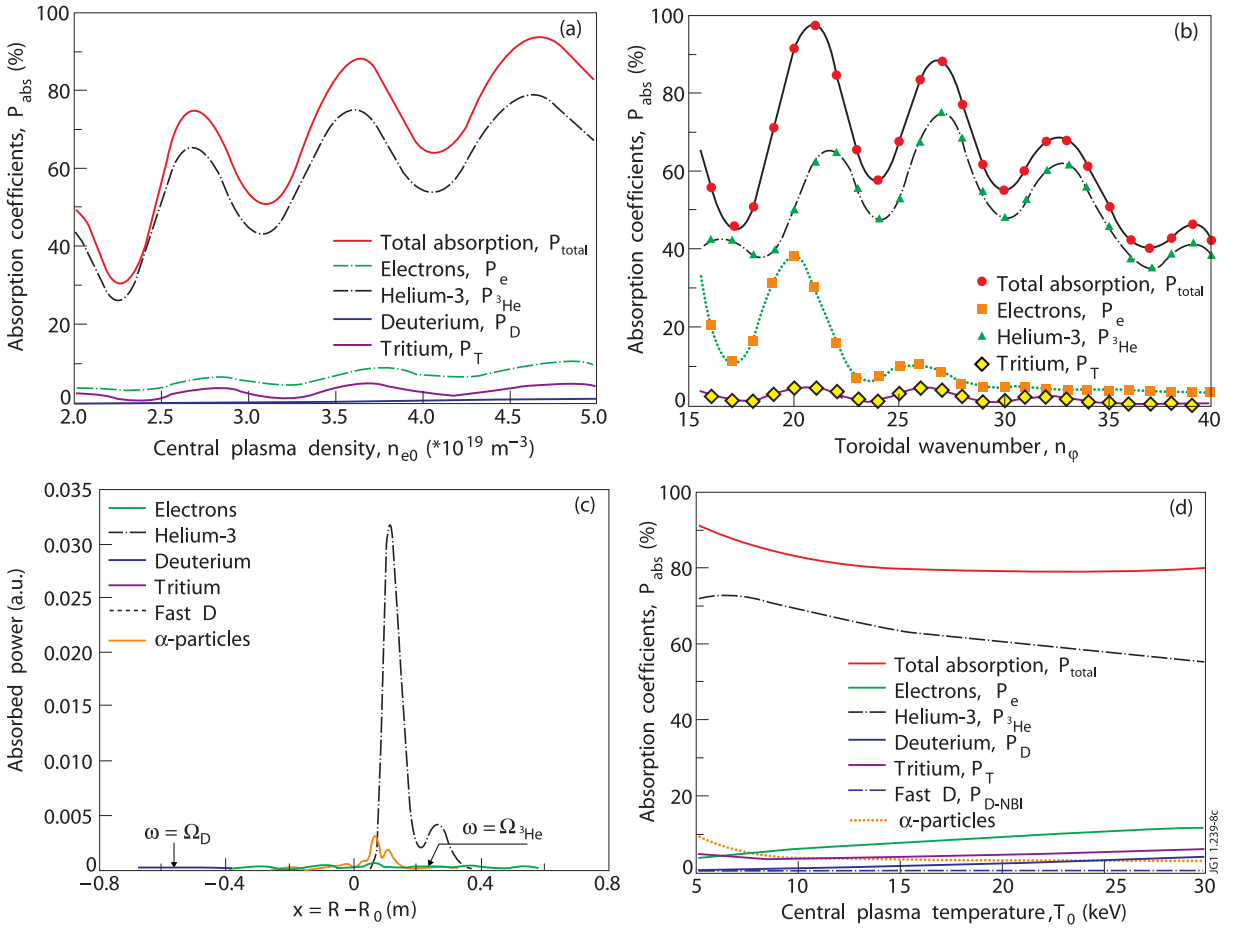

Figure 8. TOMCAT results for (^{3}He)–DT ICRH scenario, $X[^3\mathrm{He}] = 3.5\%$, T : D= 1 : 1, $n_\varphi = 27$, $f = 34$ MHz, $B_0 = 3.6$ T, $T_0 = 6$ keV. (*a*) Absorption coefficients (without fast particles) versus the central plasma density; (*b*) absorption coefficients (without fast particles) versus the toroidal wavenumber, $n_{e0} = 3.6 \times 10^{19}$ m^{-3}; (*c*) ICRH power deposition profiles (with fast particles) for $n_\varphi = 27$, $n_{e0} = 3.6 \times 10^{19}$ m^{-3}; (*d*) absorption coefficients (with fast particles) versus the central plasma temperature for $n_\varphi = 27$, $n_{e0} = 3.6 \times 10^{19}$ m^{-3}.

Our results confirm good performance of (^{3}He)–DT scenario, in which most of the RF energy is absorbed by ^{3}He minority ions with a subsequent dominant collisional transfer of the energy to the bulk ions.

Comparing the normalized absorption coefficients for D–T plasma given by TOMCAT to the results of 2D full-wave TORIC code, we showed a qualitative agreement for the heating rates predicted by the codes. However, in 2D geometry upon summing over all coupled poloidal modes, the constructive interference effect is moderated to what is expected from the 1D modelling. Also the competition between the plasma temperature and poloidal magnetic field effects important for resolving properly the converted ICW mode is outside the limits of the TOMCAT 1D description used for the scans of plasma parameters. In the experiment, the interference pattern could be further smoothened since the ICRH antenna excites a finite spectrum of the waves with different toroidal wavenumbers. Since the RF field pattern is a sensitive function of various plasma parameters (D : T ratio and impurity concentrations, plasma density and temperature, etc) which vary during discharges, it makes the control of the wave interference and its tuning to be a challenging task for the present-day experiments. Although there is experimental evidence for the enhanced mode conversion efficiency and interference effects to occur in tokamak plasmas [9, 16, 19, 22, 23], the conditions optimal for the plasma heating are commonly identified only after the experiment by making non-trivial cross-check analysis.

In D–T plasma on JET, it will be possible to perform quite accurate measurements of DT neutron rate with good time resolution, as well as DT neutron profile with good space resolution [12]. Taking into account the high sensitivity of the DT neutron yield on ion temperature, the neutron measurements could serve as a diagnostic of thermal ion heating, which is much more difficult to assess in experiments without tritium. In such a way, the use of neutron diagnostics on JET is an exciting opportunity for clarifying the efficiency of the ion heating by the RF-technique discussed in this paper.

Further improvement of the constructive interference theory should be extended for actual 2D geometry of tokamaks including the description of the mode converted ICW and accounting for the non-Maxwellian distribution functions. Possible application of the constructive interference effect to the alpha channelling problem [59] may become another important approach in increasing the fusion reactivity of D–T plasma.

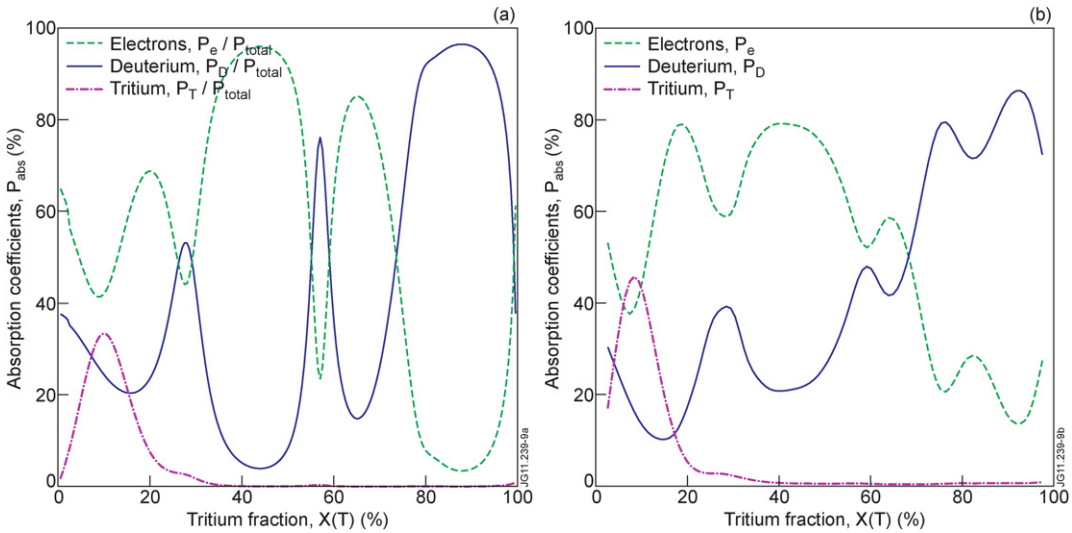

Figure A1. Comparison of TOMCAT (*a*) and TORIC (*b*) results for the absorption coefficients for the heating scenario discussed in section 2. The parameters correspond to figure 4(*a*). TOMCAT coefficients are normalized to the total double-pass absorption.

Acknowledgments

The authors are grateful to Dr M. Brambilla and Dr R. Bilato for providing the TORIC code. Ye.O. Kazakov acknowledges the financial support from the IAEA to attend the 12th IAEA Technical Meeting on Energetic Particles. This work, part-funded by the European Communities under Association Contract between EURATOM and Vetenskapsrådet, was carried out within the framework of the European Fusion Development Agreement. The views and opinions expressed herein do not necessarily reflect those of the European Commission. This work was also part-funded by the RCUK Energy Programme under grant EP/I501045. Last but not least, constructive comments of the referees are gratefully acknowledged.

Appendix A. Comparison with TORIC results

In this appendix we compare the numerical results for the heating scenario considered in section 2 (figure 4(*a*)) calculated with 1D TOMCAT code and 2D TORIC code. The TORIC code [42] has proven to be a powerful tool for the simulation and analysis of ICRH in tokamak plasmas [48, 60]. By comparing the experimental observations with TORIC modelling the ICW was identified for the first time in Alcator C-Mod [61]. TORIC has been recently used as a tool for benchmarking ICRH scenarios for ITER [62]. The code solves Maxwell's equations in an axisymmetric toroidal magnetic configuration and describes the propagation and absorption of the externally launched fast magnetosonic wave, as well as those of the IBW and ICW excited by linear MC. The ion damping is modelled at the fundamental and first harmonic cyclotron frequencies, and the Landau and transit-time (with mixed-term) damping is considered for electron absorption. TORIC relies on Fourier decomposition of the electric field components in the poloidal and toroidal directions, and uses cubic finite elements in the radial direction. More details on the TORIC code and the physics models implemented can be found in [42, 60].

For convenience, we summarize the parameters used for the simulations: $f = 23\,\mathrm{MHz}$, $B_0 = 3.6\,\mathrm{T}$, $n_\varphi = 27$, $n_{e0} = 3.0 \times 10^{19}\,\mathrm{m}^{-3}$, $T_{e0} = 7.2\,\mathrm{keV}$, $T_{i0} = 6.6\,\mathrm{keV}$. The density and temperature profiles are parametrized by the expressions $n_e(r) = (n_{e0} - n_{e1})(1 - (r/a)^2)^{k_n} + n_1$, $T(r) = (T_0 - T_1)(1 - (r/a)^2)^{k_T} + T_1$. The density is taken to be parabolic with the edge density to be 0.1 of the central value. The temperatures are assumed to have the profile factor $k_T = 1.5$ with the edge values being 0.1 of the central ones.

The scan of the double-pass absorption coefficients (excluding fast-particle populations) evaluated with TOMCAT is shown in figure 4(*a*). As mentioned in the main text, TOMCAT yields double-pass absorption coefficients whereas most of the full-wave codes assume that all RF energy is absorbed in the plasma volume. Thus, to compare TOMCAT and TORIC results it is more adequate to plot the normalized TOMCAT absorption coefficients with respect to the total double-pass absorption. These are depicted in figure A1(*a*). The corresponding TORIC results calculated for 801 radial elements and 511 poloidal modes in the truncated Fourier series are shown in figure A1(*b*).

One could see a qualitative agreement between the codes. For $X[\mathrm{D}] < 25\%$ minority ion heating is the main RF power absorption mechanism. Then, electron heating starts to dominate marking the transition to MC. One should notice the peak in the absorption by deuterium at $X[\mathrm{D}] \sim 45\%$ which corresponds to the case of the destructive interference for MC. For such conditions overall double-pass absorption coefficient is low (see figure 4(*a*)), and MH being inefficient due to very high deuterium concentration is comparable to a low electron absorption due to the destructive interference. Analogous considerations apply for the ion absorption maximum at $X[\mathrm{T}] \sim 25$–30%. However, as discussed before, in 2D geometry the wave interference is moderated comparing with results within a 1D description, and the interference patterns are less pronounced in the plasma.

Appendix B. Phase difference evaluation for MH

This appendix is devoted to addressing in more detail the wave interference for MH, particularly, by evaluating numerically

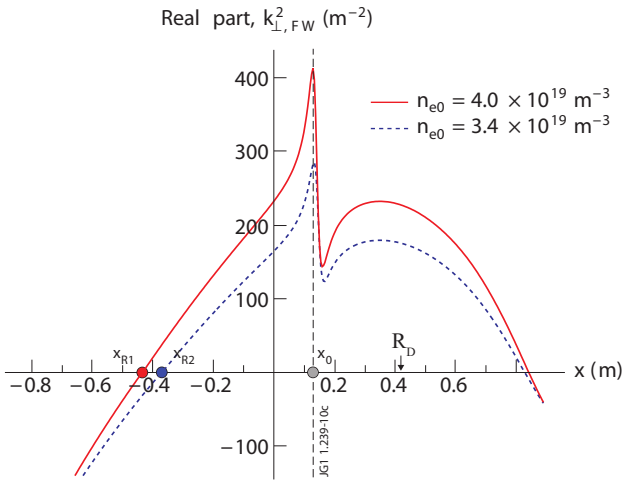

Figure B1. Dispersion of the FW corresponding to the parameters of figure 7(*a*). Two different central plasma densities are considered which represent two limiting cases of the constructive and destructive wave interference.

the phase difference for two different cases which correspond to the constructive and destructive interference, respectively. We consider the baseline heating scenario of section 5. As follows from table 1 and figure 7(*a*), the increase in double-pass ion absorption coefficient is observed at $n_{e0} = 4.0 \times 10^{19}\,\mathrm{m}^{-3}$, while for the central density $n_{e0} = 3.4 \times 10^{19}\,\mathrm{m}^{-3}$ the heating minimum is achieved indicating the destructive interference to occur. As discussed in section 4, the double-pass ion absorption coefficient is determined by the phase difference between the FW partially reflected at the region of the minority cyclotron resonance and the FW reflected from the HFS R-cutoff. This means that the phase difference $\Delta\phi$ should include—like for MC heating within the triplet configuration and two IIH resonances models [21, 25]—the term 2Φ, which describes additional phase incursion of the FW due to the double pass of the wave from the reflection point at the cyclotron layer, x_0 to R-cutoff:

$$\Phi = \int_{x_0}^{x_R} k_{\perp,\mathrm{FW}}(x)\,\mathrm{d}x. \qquad \text{(B1)}$$

Figure B1 shows the FW dispersion for the considered two cases. The position of R-cutoff in the plasma slightly changes with n_{e0} (see, table 1), as well as the FW perpendicular wavenumber is modified. For low toroidal wavenumbers it is inversely proportional to the square root of the plasma density. For the specific parameters considered the average FW wavenumber (in a region between x_0 and x_R) changes from $\bar{k}_{\perp,\mathrm{FW}} = 10.2\,\mathrm{m}^{-1}$ for the density $n_{e0} = 3.4 \times 10^{19}\,\mathrm{m}^{-3}$ to $\bar{k}_{\perp,\mathrm{FW}} = 11.9\,\mathrm{m}^{-1}$ for the density $n_{e0} = 4.0 \times 10^{19}\,\mathrm{m}^{-3}$. We have evaluated the phase integral (B1) numerically. As a reflection point x_0, we assumed a region where a sudden change in the FW dispersion occurs (figure B1). Its location actually corresponds closely to the cold-plasma hybrid resonance. However, one should note that within the hot-plasma model the typical cutoff-resonance pair is not formed for the parameters considered.

Numerical integration yields $\Phi_1 = 5.14$ and $\Phi_2 = 6.70$ for the cases corresponding to the destructive and constructive wave interference, respectively. In such a way the phase difference $\Delta\phi$ distinguishing these two cases changes by the value $2(\Phi_2 - \Phi_1)$, which is 3.11. This number is very close to π—the value expected from theory—which should divide the two limiting interference cases. This numerical result supports our arguments for the wave interference physics in MH regime and the choice of the reflection point x_0. Furthermore, we could write the total phase difference $\Delta\phi$ as the sum of the three terms [25]:

$$\Delta\phi = 2\Phi + \pi/2 - \Psi. \qquad \text{(B2)}$$

The first term in equation (B2) has already been addressed. The second term indicates the FW phase shift when it reflects at R-cutoff. The third term in equation (B2) stands for the additional FW phase shift due to the reflection at $x = x_0$. While for the MC regime this value is determined by the argument of the Stokes multiplier of the isolated cutoff-resonance pair [21, 25], for the MH regime we could not provide analytical expression for this term. By analysing numerical values for the phases Φ_1 and Φ_2 one could conclude that for the considered scenario $\Psi = -0.23\pi$.

References

[1] ITER Physics Basis Expert Group on Energetic Particles, Heating and Current Drive and ITER Physics Basis Editors 1999 Chapter 6: Plasma auxiliary heating and current drive *Nucl. Fusion* **39** 2495–539
[2] Lamalle P.U. *et al* 2009 *Proc. 18th Topical Conf. on RF Power in Plasmas (Gent, Belgium, 24–26 June 2009) AIP Conf. Proc.* **1187** 265–8
[3] Becoulet A. 1996 *Plasma Phys. Control. Fusion* **38** A1–11
[4] Longinov A.V. and Stepanov K.N. 1992 *High-Frequency Plasma Heating* ed A G Litvak (New York: AIP) pp 93–238
[5] Mayoral M.-L. *et al* 2006 *Nucl. Fusion* **46** S550–63
[6] Mantica P. *et al* 2006 *Phys. Rev. Lett.* **96** 095002
[7] JET and TFTR teams (presented by Start D.F.H.) 1998 *Plasma Phys. Control Fusion* **40** A87–103
[8] Phillips C.K. *et al* 1999 *Proc. 13th Topical Conf. on RF Power in Plasmas (Annapolis, MD, 12–14 April 1999) AIP Conf. Proc.* **485** 69–78
[9] Phillips C.K. *et al* 1995 *Phys. Plasmas* **2** 2427–34
[10] Wilson J.R. *et al* 1995 *Phys. Rev. Lett.* **75** 842–5
[11] Start D.F.H. *et al* 1999 *Nucl. Fusion* **39** 321–36
[12] Start D.F.H. *et al* 1998 *Phys. Rev. Lett.* **80** 4681–4
[13] JET team (prepared by Cottrell G.A. and Rimini F.G.) 1999 *Nucl. Fusion* **39** 2025–32
[14] Bergeaud V. *et al* 2000 *Nucl. Fusion* **40** 35–51
[15] Van Eester D. *et al* 2002 *Nucl. Fusion* **42** 310–28
[16] Eriksson L.-G. *et al* 1999 *Nucl. Fusion* **39** 337–52
[17] Eriksson L.-G. and Hellsten T. 1995 *Phys. Scr.* **52** 70–9
[18] Budden K.G. 1985 *The Propagation of Radio Waves* (Cambridge: Cambridge University Press)
[19] Majeski R. *et al* 1996 *Phys. Rev. Lett.* **76** 764–7
[20] Majeski R. *et al* 1994 *Phys. Rev. Lett.* **73** 2204–7
[21] Fuchs V. *et al* 1995 *Phys. Plasmas* **2** 1637–47
[22] Van Eester D. *et al* 2009 *Plasma Phys. Control. Fusion* **51** 044007
[23] Van Eester D. *et al* 2012 *Plasma Phys. Control. Fusion* **54** 074009
[24] Kazakov Ye.O. *et al* 2008 *Problems of Atomic Science and Technology* #4, 99–103 http://vant.kipt.Kharkov.ua/ARTICLE/VANT_2008_4/article_2008_4_99.pdf
[25] Kazakov Ye.O. *et al* 2010 *Plasma Phys. Control. Fusion* **52** 115006
[26] Hellsten T. *et al* 1985 *Nucl. Fusion* **25** 99–105

[27] Koch R. 1991 *Phys. Lett.* A **157** 399–405
[28] Hedin J. *et al* 1998 *Plasma Phys. Control. Fusion* **40** 1085–95
[29] Stix T.H. 1992 *Waves in Plasmas* (New York: AIP)
[30] Perkins F. 1977 *Nucl. Fusion* **17** 1197–224
[31] Jaeger E.F. *et al* 2003 *Phys. Rev. Lett.* **90** 195001
[32] Wright J.C. *et al* 2004 *Phys. Plasmas* **11** 2473–9
[33] Parisot A. *et al* 2005 *Proc. 16th Topical Conf. on RF Power in Plasmas (Park City, UT, 11–13 April 2005) AIP Conf. Proc.* **787** 138–41
[34] Mantsinen M.J. *et al* 2004 *Nucl. Fusion* **44** 33–46
[35] Lin Y. *et al* 2009 *Phys. Plasmas* **16** 056102
[36] Lamalle P.U. *et al* 2006 *Nucl. Fusion* **46** 391–400
[37] Bilato R. *et al* 2005 *Nucl. Fusion* **45** L5–7
[38] Messiaen A. and Weynants R. 2011 *Plasma Phys. Control. Fusion* **53** 085020
[39] Kazakov Ye.O. *et al* 2008 *Ukr. J. Phys.* **53** 443–50
[40] Van Eester D. and Koch R. 1998 *Plasma Phys. Control. Fusion* **40** 1949–75
[41] Hedin J. *et al* 2002 *Nucl. Fusion* **42** 527–40
[42] Brambilla M. 1999 *Plasma Phys. Control. Fusion* **41** 1–34
[43] Jaeger E.F. *et al* 2008 *Phys. Plasmas* **15** 072513
[44] Ćirić D. *et al* 2007 *Fusion Eng. Des.* **82** 610–8
[45] Hellsten T. *et al* 2004 *Nucl. Fusion* **44** 892–908
[46] Jaeger E.F. *et al* 2006 *Phys. Plasmas* **13** 056101
[47] Lerche E. *et al* 2009 *Plasma Phys. Control. Fusion* **51** 044006
[48] Bilato R. *et al* 2011 *Nucl. Fusion* **51** 103034
[49] Darrow D.S. *et al* 1996 *Nucl. Fusion* **36** 509–13
[50] Choi M. *et al* 2003 *Proc. 15RF Topical Conf. on RF Power in Plasmas (Moran, WY, 19–21 May 2003) AIP Conf. Proc.* **694** 86–9
[51] Krasilnikov A.V. *et al* 2009 *Plasma Phys. Control. Fusion* **51** 044005
[52] Kiptily V.G. *et al* 2009 *Nucl. Fusion* **49** 065030
[53] Sharapov S.E. *et al* 1999 *Nucl. Fusion* **39** 373–88
[54] Wesson J. 2004 *Tokamaks* (Oxford: Clarendon)
[55] Stix T.H. 1975 *Nucl. Fusion* **15** 737–54
[56] Bhatnagar V.P. *et al* 1993 *Nucl. Fusion* **33** 83–99
[57] Swanson D.G. 1995 *Rev. Mod. Phys.* **67** 837–62
[58] Chow C. *et al* 1990 *Phys. Fluids* B **2** 2185–90
[59] Fisch N.J. and Herrmann M.C. 1994 *Nucl. Fusion* **34** 1541–56
[60] Brambilla M. and Bilato R. 2009 *Nucl. Fusion* **49** 085004
[61] Nelson-Melby E. *et al* 2003 *Phys. Rev. Lett.* **90** 155004
[62] Budny R.V. *et al* 2012 *Nucl. Fusion* **52** 023023